Food Chemistry 460 (2024) 140720

Contents lists available at ScienceDirect

Food Chemistry

journal homepage: www.elsevier.com/locate/foodchem

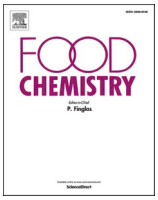

Biointerfacial supramolecular self-assembly of whey protein isolate nanofibrils on probiotic surface to enhance survival and application to 3D printing dysphagia foods

Ye Zhang [1], Yexuan Wang [1], Xiaohan Dai, Ying Li, Bin Jiang, Dongmei Li, Chunhong Liu [*], Zhibiao Feng [*]

Department of Chemistry, College of Arts and Sciences, Northeast Agricultural University, Harbin 150030, China

ARTICLE INFO

Keywords:
Whey protein isolate nanofibrils
Biointerfacial supramolecular self-assemble
3D printing
Dysphagia foods
Lactiplantibacillus plantarum

ABSTRACT

Personalized three-dimensional (3D) printed foods rich in probiotics were investigated. *Lactiplantibacillus plantarum* (Lp), as a representative of probiotics, was used to investigate the 3D printing of probiotic-rich dysphagia foods. Here, whey protein isolate nanofibrils (WPNFs) were coated and anchored on bacterial surfaces via biointerfacial supramolecular self-assembly, providing protection against environmental stress and the 3D printing process. The optimized composite gels consisting of High acyl gellan gum (0.25 g), whey protein isolate (1.25 g), fructooligosaccharides (0.75 g), Lp-WPNFs-Glyceryl tributyrate emulsion (Φ = 40%, 3.75 mL) can realize 3D printing, and exhibit high resolution, and stable shape. The viable cell count is higher than 8.0 log CFU/g. They are particularly suitable for people with dysphagia and are classified as level 5-minced & moist in the international dysphagia diet standardization initiative framework. The results provide new insights into the development of WPNFs-coating on bacterial surfaces to deliver probiotics and 3D printed food rich in probiotics.

1. Introduction

Dysphagia is an age-related syndrome that reduces a patient's ability to ingest food, making it difficult to swallow foods of normal size and texture (Liu, Wang, et al., 2024). This limits the patient's dietary choices and prevents them from eating foods that require a lot of chewing, and the reduced food and nutrient intake can lead to dehydration and malnutrition (Dick et al., 2020). Probiotics, as live microorganisms, provide multiple health benefits when consumed at sufficiently high levels, with a minimum of 10^6–10^7 colony forming units (CFU)/g recommended in products (Liu et al., 2018; Zhang et al., 2022). Artificial ingesting probiotics can significantly alter the composition of the intestinal flora, boost the immune system in humans, promote and maintain gastrointestinal peristalsis, reduce inflammation, and act as a preventive measure against cancer (Kwak et al., 2022; Mazziotta et al., 2023; Sun et al., 2023; Yadav et al., 2022). Probiotic-rich diets are beneficial for keeping the body healthy, especially for the elderly with dysphagia. However, probiotics are sensitive to various environmental factors as well as food handling and processing such as temperature, pH levels, product matrix, and the mechanical shear at the nozzle during 3D printing extrusion, all of which can lead to decreased bacterial viability (Yoha et al., 2021; Zhang et al., 2022).

Three-dimensional (3D) printing, as an emerging technology, offers many advantages, including personalized nutrition, structural customization and simplified supply chain (Xu et al., 2023). Personalized three-dimensional (3D) printed foods enriched with attractive appearance and tailored nutritional content can prevent the risk of reduced appetite and malnutrition in people with dysphagia (Lorenz et al., 2022). In recent years, studies have been conducted to investigate the 3D printing properties of different probiotic-enriched food materials, including Kefir gels (Ok et al., 2024), Pickering emulsion gel stabilized by tea protein/xanthan gum (Xu et al., 2023), custard cream (Cai et al., 2023), mashed potatoes (Liu, Li, et al., 2020; Sun et al., 2022), and starch-Based Gel (Chen, Teng, Zhang, Mujumdar, and Li, 2023). However, few studies have addressed probiotic-enriched 3D printed dysphagia foods. This is mainly due to the sensitivity of probiotics to the 3D printing process and the special needs of dysphagia foods that should be soft enough for chewing and safe for swallowing (Qiu et al., 2023).

* Corresponding author at: Department of Applied Chemistry, College of Arts and Sciences, Northeast Agricultural University, Harbin, Heilongjiang 150030, China.
E-mail addresses: liuchunhong@neau.edu.cn (C. Liu), fengzhibiao@neau.edu.cn (Z. Feng).

[1] These authors contributed to the work equally and should be regarded as co-first authors.

https://doi.org/10.1016/j.foodchem.2024.140720
Received 2 April 2024; Received in revised form 14 July 2024; Accepted 29 July 2024
Available online 2 August 2024

Encapsulation using synthetic materials and chemical based surface modification has been explored to enhance the stability and viability of probiotics and exhibits great potential in various food and biomedical applications (Cao et al., 2019; Kim et al., 2019; Lin et al., 2023). Wrapping an extra lipid membrane around the bacteria through bio-interfacial supramolecular self-assembly can help the bacteria to cope with stress and generate super gut microbes (Cao et al., 2019). Protein nanofibrils (PNFs) are amyloid-like structures with diameters of about 1–10 nm and lengths of several micrometers (1–10 μm), that are self-assembled from various original proteins (Cao & Mezzenga, 2019; Meng et al., 2022; Wang, Guo, et al., 2023; Yang et al., 2022). Whey protein isolate nanofibrils (WPNFs) have an isoelectric point of about 5.5, and thus are generally positively charged at pH 2.0 (Fan et al., 2021). Teichoic acid on the surface of *Lactiplantibacillus plantarum* causes the surface of the bacterium to be negatively charged (Stepnaya et al., 2004). The electrostatic interaction between a natural cationic polysaccharide and bacteria is often used to protect the stability of probiotics (Yuan et al., 2022). WPNFs are anisotropy, large aspect ratio and mechanical strength have been engineered into different delivery systems, such as emulsions, gels, microcapsules, and complexes (An et al., 2022; Gao et al., 2017; Liu, Bhandari, and Zhang, 2020; Wei & Huang, 2019). Therefore, we hypothesized that WPNFs with self-assembly and post-self-assembly capabilities (Liu, Chen, et al., 2024) could self-assemble on the bacterial surface under electrostatic interactions, thus acting as a barrier and safeguard to protect the viability.

Glyceryl tributyrate (GTB) facilitates probiotic colonization in the intestine and enhances the intestinal barrier function, and has been approved as a non-toxic and well tolerated additive, widely used in food and pharmaceutical fields (Cao et al., 2024; Liu et al., 2022). GTB, as a precursor of butyric acid, can degrade and release butyric acid in the intestine, maintaining intestinal bacterial balance (Cao et al., 2024; Kang et al., 2012; Liu et al., 2022). Nevertheless, GTB has unpleasant odor and poor solubility, and it is easily degraded and absorbed in the upper gastrointestinal tract, making it difficult to reach the colon at a physiologically efficacious concentration (Donovan et al., 2017). Preparation of GTB as an emulsion is the most common method for its targeted delivery (Cao et al., 2024). WPNFs are good Pickering emulsion stabilizers (Liu, Chen, et al., 2024) for protecting and dispersing GTB into Pickering emulsions.

Appropriate protection systems have provide high encapsulation efficiency, viability and storability (Liu et al., 2018). High acyl gellan gum (HG) exhibits excellent performance due to its non-toxicity, biocompatibility, resistance to acid stress and heat, and optical (transparent gel), especially as it has a high gelation temperature (Bian et al., 2024; Chen et al., 2017). Moreover, HG can form soft elastic hydrogels and is widely used as a thickener in the food industry (Akkineni et al., 2022). Whey protein isolate (WPI) and HG can form a mixed gel in response to heat and be used for 3D printing (Oliveira et al., 2020). Protein-polysaccharide gels have been shown to have significant and unique properties in food formulations, and the aggregate properties of the network can be altered by adjusting the ratio of protein to polysaccharide, making them suitable for different food designs (Guo et al., 2023).

Combining prebiotics with probiotic bacteria can be a great way to achieve health enhancing and synergistic effects (Nezamdoost-Sani et al., 2023; Yoha et al., 2021). Here, WPNFs was initially self-assembly onto the bacterial surface for protection, composite hydrogel with HG and WPI as carrier matrix, as well as GTB and FOS as prebiotic, to further realize the combination of prebiotics and probiotics for 3D printing dysphagia foods. Extrusion-based 3D printing was chosen because it is the most popular food printing approach and is particularly suitable for semi-solid materials. 3D printing of probiotic-enriched easy-to-swallow composite hydrogels could meet the probiotic needs of people with dysphagia. This study will be the foundation for 3D printing probiotic-enriched foods with personalized shapes and nutrients.

2. Materials and methods

2.1. Materials and chemicals

Whey protein isolates (WPI) containing >93% protein was purchased from Hilmar Industries (Hilmar, CA, USA). Nile red and Nile blue dyes were bought from Aladdin Biochemical Technology Co. Ltd. (Shanghai, China). 4′,6-diamidino-2-phenylindole (DAPI) was bought from Boao Tuoda Technology Co., Ltd. (Beijing, China). MRS (De Man Rogosa and Sharpes) agar (GM641) was procured from Guangdong Huankai Microbial Technology Co., Ltd. (China). The other chemicals were analytical grade in the experiments and were purchased from Aladdin Biochemical Technology Co. Ltd. (Shanghai, China). *Lactiplantibacillus plantarum* 1.0665 (Lp) was kindly provided by the laboratory of the College of Food Science, Northeast Agricultural University, China.

2.2. Preparation and characterization of WPNFs

2.2.1. Preparation of WPNFs

WPNFs were prepared according to the previous method of Han et al. (2023). Briefly, the pH of a 5.0% WPI solution was adjusted to 2.0, followed by magnetic stirring for 30 min, centrifugation at 9000 r/min and 4 °C for 15 min. The supernatant was then filtered with a 0.45-μm pore size fibrous membrane, and the filtrate was incubated in a water bath at 80 °C and 220 rpm for 10 h to obtain a WPNFs solution (Han et al., 2023).

2.2.2. Characterization of WPNFs by transmission electron microscopy (TEM)

The obtained WPNFs solution was diluted 40-fold with HCl solution of pH 2.0 and then filtered by centrifugation using 100 kDa ultrafiltration centrifuge tubes, in which the samples had to be eluted three times. A drop of diluted solution was transferred onto a carbon-coated copper grid and stood for 15 min. The sample was then stained with 2% uranyl acetate for 8 min. The microscopic morphology of the fibrils was observed using a transmission electron microscope (HT-7800, Hitachi Company, Japan).

2.3. Preparation and viability of the probiotic bacterium

One colony of *L. plantarum* was cultured in MRS liquid medium at 30 °C for 24 h, and then the bacterial solution was centrifuged at 4000 rpm for 10 min at 4 °C. The bacterial cell was resuspended with a 12.5 mmol/L $CaCl_2$ solution and stored at 4 °C.

The survival of the probiotic bacterium was determined using 10-fold serial dilutions and then cultured on MRS agar medium at 37 °C for 48 h (Cai et al., 2023; Yoha et al., 2021). The colony-forming units (CFU/g) were calculated by eq. (1).

$$N = \frac{\Sigma C}{(n_1 + 0.1n_2)d} \quad (1)$$

where N is the cell viability (in CFU/g), ΣC is the total number of colonies in all plates, n_1 is the count of plates in lower dilution, n_2 is the count of plates in the next higher dilution, d is dilution factor.

2.4. Preparation and characterization of WPNFs coated probiotic bacterium

2.4.1. Preparation of WPNFs coated probiotic bacterium

The bacterial cells were obtained by centrifugation of the bacterial solution at 4000 r/min for 10 min. After the bacterial cells were washed three times and suspended in a 12.5 mmol/L $CaCl_2$ solution, the WPNFs solution was added to the bacterial solution at a ratio of 49:1. The mixture was incubated for 1 h at room temperature to allow the WPNFs

to self-assemble and coat on the bacterial surface. The coated bacteria were defined as Lp-WPNFs, and the uncoated bacteria (Lp) were used as the control.

2.4.2. Transmission electron microscopy (TEM)

The microstructures of bacteria in Lp and Lp-WPNFs were observed by transmission electron microscopy (HT7800, HITACHI, Japan). Briefly, 100 μL of the samples were placed on a carbon-coated copper mesh and stood for 90 min. The sample was then stained with 2% uranyl acetate for 8 min.

2.4.3. Particle size and zeta potential determination

A laser particle sizer (SYNC, Microtrac Inc., USA) was employed to determine the particle size and Zeta potential (ζ) of the samples (Jiang et al., 2024). The samples were diluted 100 times with 12.5 mmol/L $CaCl_2$ solution, and then tested at 25 °C. The refractive indices of the particles were 1.46, and that of the dispersed phase was 1.33.

2.5. Preparation and characterization of GTB emulsion loaded with Lp

2.5.1. Preparation of GTB emulsion loaded with Lp

Different fractions of GTB were added to the Lp-WPNFs solution, and then the mixture was homogenized at 20000 rpm for 2 min with hand-held homogenizer (F6/10, Fuguang Precision Instrument Co., Ltd., China). The obtained Pickering emulsion is defined as Lp-WPNFs-GTB.

2.5.2. Confocal laser scanning microscopy (CLSM)

The microstructure of Lp-WPNFs-GTB was observed using CLSM (TCS SP8, Leica Corporation, Germany). The GTB was stained with Nile Red solution (0.1% *w/v* in ethanol) and detected by excitation at 488 nm. The WPNFs and WPI were stained with Nile blue (0.1% w/v in ethanol) and detected by excitation at 633 nm. The bacteria were stained with DAPI (0.1% *w/v*) and detected by excitation at 405 nm.

2.5.3. Viability analysis of Lp-WPNFs-GTB

To verify the protective effects of probiotic in Lp-WPNFs and Lp-WPNF-GTB under different stimulation conditions, the samples were cultured at 37 °C and 60 °C for 2 h, and at pH 2.0 and 11.0 for 2 h. Before and after exposure to heat treatment, viable cell counts were performed on MRS agar by spread plate technique. The survival rate of the probiotic was calculated by eq. (2).

$$\text{survival rate} = \frac{lgN_1}{lgN_0} \times 100\% \quad (2)$$

where N_1 is the number of colonies after the stress treatment, N_0 is the colonies in the before the stress treatment.

2.6. Preparation and characterization of 3D printing ink

2.6.1. Formulation of 3D printing ink

HG, WPI, FOS, and water were mixed according to the ratio in Table 1 and stirred in a water bath at 80 °C for 15 min. The mixture was cooled to 45 °C, which is the temperature of the extrusion cavity. Lp-WPNFs-GTB was then added to the mixture and stirred evenly to obtain the probiotic-loaded 3D printing ink.

Table 1
Composition of the studied CHs' formulations.

Formulation	Ingredients				
	HG (g)	WPI (g)	FOS (g)	Lp-WPNFs-GTB (mL)	H_2O (mL)
CH1	0.20	1.25	0.75	3.75	25.00
CH2	0.25	1.25	0.75	3.75	25.00
CH3	0.30	1.25	0.75	3.75	25.00
CH4	0.25	2.50	0.75	3.75	25.00
CH5	0.25	3.75	0.75	3.75	25.00
CH6	0.25	1.25	0.25	3.75	25.00
CH7	0.25	1.25	1.25	3.75	25.00
CH8	0.25	1.25	0.75	2.50	25.00
CH9	0.25	1.25	0.75	5.00	25.00

2.6.2. Rheological properties

The rheological characteristics of the 3D printing ink were assessed using a rheometer (Brookfield RSO CTX, USA) with the method of Liu, et al. (Liu et al., 2023). The equilibration time was set to 7 min, the shear rate was set to 0.1–100 s^{-1}, and the scanning frequency was set to 1.0 Hz. The frequency scanning parameter was set to strain of 0.1%, and the scanning frequency ranged from 0.1 to 15 Hz. Each measurement was conducted at 25 °C.

2.6.3. Low field nuclear magnetic resonance (LF-NMR) analysis

A MesoMR23-060H-I NMR spectrometer (Suzhou Niumag Analytical In-strument Co., Suzhou, China) was employed to analyze the proton relaxation time of samples. T_2 was determined at a frequency field of 20 MHz. A CPMG pulse sequence was used with the following pulse parameters: waiting time (T_W) = 1500 ms, interval between two peaks (T_E) = 0.5 ms, number of identified points (NECH) = 1500, interval between points (S_W) = 100 kHz, and the number of scans (N_S) = 8. T_2 distribution curves were established using logarithmic coordinates (Zhong et al., 2022).

2.6.4. Textural profile analysis

The textural properties of the composite hydrogels were analyzed using a texture analyzer (TA.XT PlusC, SMS, UK) with texture profile analysis (TPA) mode. A P/0.5 probe was selected to test the composite hydrogels for three compression cycles. The probe entry distance was set to 10 mm, the pre-test speed, the mid-determination probe speed and the post-determination probe speed were set to 1 mm/s, the hold time to 5 s, the trigger force to Auto-5 g. Measurements were carried out at 25 °C (Wang, Guo, et al., 2023). Hardness, cohesiveness, adhesiveness and springiness were recorded in three replicates.

2.7. 3D printing probiotic-loaded composite hydrogel (CH)

2.7.1. 3D printing process

3D printing was performed using an extrusion-based 3D printer (Wiilboox Sweetin, Wiiboox, Nanjing, China). CAD software (AutoCAD; Autodesk Inc., San Rafael, CA) was used for different designs to model and convert to STL files. A CAD-controlled xyz-motion control system was applied to guide the nozzle position and enable the deposition of 3D structures in a layer-by-layer approach (Wang, Guo, et al., 2023). The 3D printing parameters were set as follows: filling density 100%, nozzle diameter 0.84 mm, extrusion cavity temperature 45 °C and print speed 20 mm/s.

2.7.2. Survival rate affected by 3D printing

For cell reactivation, 1 g sample and 1 ml of sterile saline (0.85%) were added to a sterile tube, and then incubated on an orbital shaker at 37 °C and 100 rpm for 30 min. The cell viability of the probiotics was determined by the standard plate count method as described in section 2.3. The survival rate of the probiotic was calculated by eq. (2). Where N_1 is the number of colonies after 3D printing process, N_0 is the colonies in the before 3D printing process. The other procedures were the same, but Lp not coated with WPNFs was used as a control.

2.7.3. International dysphagia diet standardization initiative (IDDSI) tests

In the IDDSI test, the texture levels of easy-to-swallow foods are divided into eight levels, from 0 to 7 (Liu et al., 2023; Wang, Zhang, et al., 2023). Within IDDSI, the 3D printed cubes (edge length 2.0 cm) were tested by fork pressure test and spoon tilt test to evaluate their hardness and adhesiveness. The fork pressure test was performed by applying thumb pressure with a fork to the top surface of the sample and

observing the deformation behavior. The spoon tilt test was performed by scooping a teaspoonful of the sample, and then gradually tilting the spoon.

2.8. Statistical analysis

Origin 8.0 was used for graphing. DPS 7.05 was used for data analysis. The experimental processing was repeated for 3 times, and the data were expressed as mean ± standard deviation. The significant difference was considered when $p < 0.05$ with Duncan's test.

3. Results and discussion

3.1. Characterization of Lp-WPNFs

3.1.1. Microscopic morphology of WPNFs and Lp-WPNFs

The TEM was chosen to investigate the microstructure of WPNFs, Lp and Lp-WPNFs (Fig. 1). The WPNFs, obtained from WPI incubated at 80 °C and pH 2.0 for 10 h, showed an amyloid-like structure with a large aspect ratio (Fig. 1a). In our previous study it was confirmed that the length of WPNFs was about 10 μm, the diameter was about 10 nm (Liu, Chen, et al., 2024). Fibrillation endows WPNFs with improved nanomechanical properties, excluded volume and the ability to reduce interfacial tension, allowing them to self-assemble and post-self-assemble at the oil-water interface to form ultra-stable Pickering emulsions (An et al., 2022; Kamada et al., 2022; Liu, Chen, et al., 2024; Yang et al., 2022).

TEM images showed that the surface of the bacteria had visibly coated with WPNFs (Fig. 1c and d), which contrasted significantly with the smooth edges of the uncoated bacteria (Fig. 1b). The solution was diluted to a higher multiple (10-fold) to observe the coating of WPNFs on the surface of Lp, as shown in Fig. 1d. There was no reduction of WPNFs on the bacterial surface after dilution, indicating that the WPNFs were successfully coated and anchored on the bacterial surface. This is mainly due to the electrostatic interaction between the bacterial surface and WPNFs, where the bacterial surface is negatively charged due to the teichoic acid in the cell wall (Han et al., 2024; Stepnaya et al., 2004), and WPNFs are positively charged at pH 2.0 (Zhang et al., 2020). Similar results were obtained with biocompatible lipids and soy lecithin with cholesterol, which could coat bacteria via biointerfacial supramolecular self-assembly to improve their survival under various extreme conditions, such as strong acids and alkalis, simulated gastric and intestinal fluids eta (Cao et al., 2019; Han et al., 2024). Unlike biocompatible lipids, WPNFs are proteins, and this is the first study of proteins being used to coat and protect bacteria via biointerfacial supramolecular self-assembly. WPNFs anchored on the bacterial surface can form a physical barrier, enhancing their rigidity and limiting their aggregation, as was subsequently demonstrated.

3.1.2. Particle size and zeta potential analysis of Lp-WPNFs

The average particle size and Zeta potential are shown in Fig. 2. The

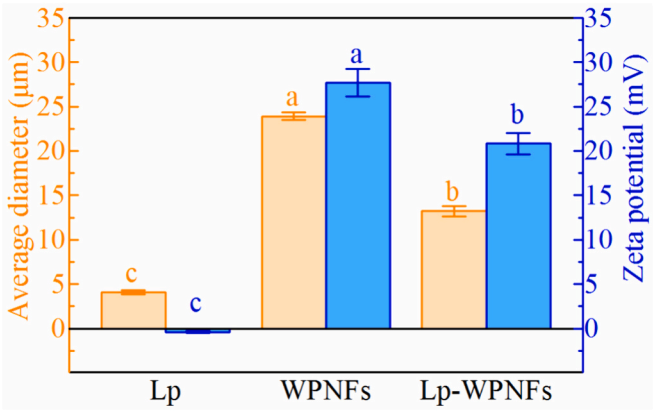

Fig. 2. Average particle sizes and Zeta potential of Lp, WPNFs and Lp-WPNFs. Superscript letters indicate significant differences of $p < 0.05$.

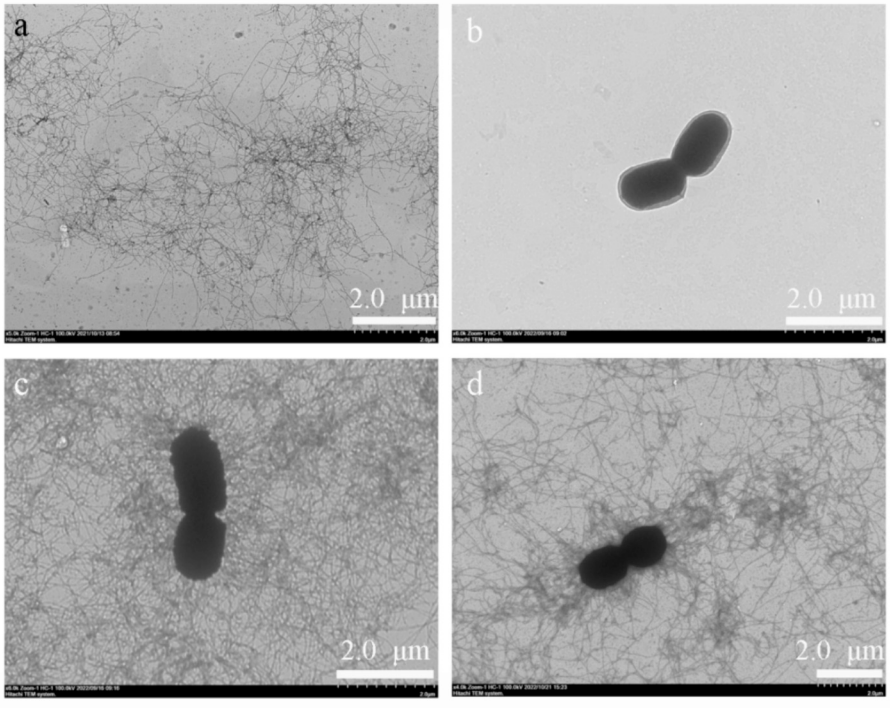

Fig. 1. TEM images of WPNFs, uncoated bacteria and Lp-WPNFs, respectively. (a) WPNFs, obtained from WPI incubated at 80 °C and pH 2.0 for 10 h, (b) uncoated bacteria, (c) 5-fold dilution of Lp-WPNFs, (d) 10-fold dilution of Lp-WPNFs. The insert scale bar is represented 2.0 μm.

average particle size of Lp-WPNFs was larger than that of uncoated bacteria. This is another evidence of WPNFs were successfully coated onto the bacterial surface. What seems unusual in the Fig. 2 was that the particle size of WPNFs was larger than that of Lp-WPNFs, mainly because the light scattering method for particle size is not perfect for the fibrous structures, but more suitable for analyzing spherical particles such as bacteria or emulsions. This method is often used to analyze the changes in the formation process of PNFs, and it should be noted that the average particle size here was not its length or diameter. These results demonstrate that WPNFs self-assembly onto bacteria surface via bio-interfacial supramolecular self-assembly is general, simple and highly efficient.

The Zeta potential can describe the electrostatic interactions between charged particles, and the higher the Zeta potential, the stronger the electrostatic repulsion, which can keep the particles at an appropriate distance from each other and prevent aggregation. The Zeta potential of Lp was -0.38 ± 0.09 mV due to the presence of teichoic acid on its surface (Stepnaya et al., 2004). The Zeta potential of Lp-WPNFs was 20.82 ± 1.23 mV, which was slightly lower than that of WPNFs of 27.68 ± 1.52 mV, due to the fact that WPNFs were anchored and coated on the negatively charged bacterial surface. The increased Zeta potential would be able to promote bacterial dispersion in solution and prevent aggregation. It is believed that the adhesion capacity of the bacteria cells to intestinal epithelial cells is affected by the auto-aggregation of probiotic strains (Ramos et al., 2013). Therefore, it can be inferred that the increased Zeta potential is beneficial for the effective utilization of probiotics.

3.2. Characterization of Lp-WPNFs-GTB emulsion

3.2.1. The stability of Lp-WPNFs-GTB emulsion

Lp-WPNFs-GTB, a Pickering emulsion, was obtained by homogenizing the mixture of Lp-WPNFs and GTB. The appearance of the Pickering emulsions with various internal phase fractions is shown in Fig. 3. When the internal phase fraction was low ($\Phi = 20\%$), significant serum layer appearance was observed in both Lp-WPNFs-GTB and Lp-WPI-GTB. As the internal phase fraction increased to $\Phi = 40\%$, the serum layer of Lp-WPNFs-GTB disappeared, but a small amount of serum layer could be observed in Lp-WPI-GTB. This is mainly due to the better emulsifying properties of WPNFs compared to WPI, which is consistent with the research results of Yang et al. (2022).

3.2.2. The microstructure of Lp-WPNFs-GTB emulsions

The distribution of bacterial cells, GTB and WPNFs in the Lp-WPNFs-GTB emulsion analyzed by CLSM is shown in Fig. 4. The bacterial cells stained with DAPI showed bright blue fluorescence (Fig. 4 **a**), GTB stained with Nile Red showed red fluorescence (Fig. 4 **b**), WPNFs stained with Nile Blue showed green fluorescence (Fig. 4 **c**). The superimposed effect of bacterial cells and GTB (Fig. 4 **d**) showed that the bacteria were distributed in the continuous aqueous phase between oil droplets. The superimposed effect of bacterial cells and WPNFs (Fig. 4 **e**) showed that the WPNFs were successfully coated on the bacterial surface; and the rest of the WPNFs could automatically disperse at the oil-water interface

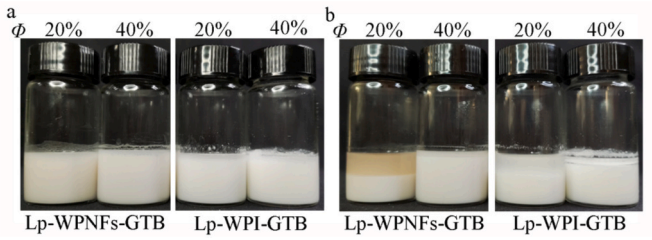

Fig. 3. The appearance of Lp-WPNFs-GTB and Lp-WPI-GTB with different oil phase fractions at different storage times. (a) 0 day, (b) 7 day.

to form Pickering emulsion. This is consistent with the analysis results of Pickering emulsion stability (Fig. 3), this is consistent with the findings of Yang et al. (Yang et al., 2024), An, et al. (An et al., 2023) and Liu et al. (Liu, Bhandari, and Zhang, 2020). WPNFs have good emulsifying activity and stability (Liu, Chen, et al., 2024; Yang et al., 2022), so it is not necessary to add any other emulsifier to form a stable Pickering emulsion. To sum up, these results demonstrated the successful preparation of WPNFs-coated probiotics and WPNFs-stabilized Pickering emulsions.

3.2.3. Viability of probiotic in Lp-WPNF and Lp-WPNFs-GTB

The number of viable microorganisms is closely related to the effectiveness of probiotic supplements (Guo et al., 2022). Therefore, it is necessary to clarify the contribution of each component in maintaining bacterial survival rate, which is shown in Fig. 5a. As can be seen, storage time showed a significant effect on probiotic viability. In all samples, the survival rate of bacteria decreased during the storage time at 4 °C. However, the survival rate of probiotics in Lp-WPNFs and Lp-WPNFs-GTB was higher than that of uncoated bacteria at the same storage time, suggesting that the coating of WPNFs had a significant effect on improving the viability of probiotics; whereas the survival rates were not significantly different between Lp-WPNFs-GTB and Lp-WPNFs, suggesting that GTB had no significant effect on the survival rate of bacteria in Pickering emulsion. It could be concluded that the WPNFs coating on the bacterial surface had a protective effect on the bacteria which significantly improved the storage stability of the bacteria at 4 °C. Many similar studies have been reported that encapsulated and coated probiotics are well protected during storage and digestion (Guo et al., 2022; Yoha et al., 2021; Yuan et al., 2022).

Heat processing is one of the main processes in the 3D printing and can reduce the viability of bacteria (Abbasi et al., 2023). The effect of heating processes on the survival rate of probiotics in Lp, Lp-WPNFs and Lp-WPNFs-GTB is shown in Fig. 5b. Regardless of the stress treatment, a significant loss of activity was observed in Lp, suggesting that the bacteria have a low capacity for stress resistance. Similar results showed that unencapsulated L. *plantarum* showed no viability at 72 °C after only 2 min (Abbasi et al., 2023). Free bacteria were also inactivated after exposure to a temperature of 60 °C for 2 h, but the survival rate of probiotics in Lp-WPNFs and Lp-WPNFs-GTB could still reach 22.12% and 61.24%, respectively. This indicated that WPNFs coated on the bacterial surface significantly improved its thermal stability, and the formation of the emulsion system also provided some assistance in the survival of the probiotics.

The survival rates of the probiotics in Lp, Lp-WPNFs and Lp-WPNFs-GTB at pH 2.0 and 11.0 are shown in Fig. 5b. The highest decrease in survival rate was observed in Lp, followed by Lp-WPNFs-GTB and finally Lp-WPNFs at either pH 2.0 or 11.0. The survival rate of the bacteria in Lp-WPNFs and Lp-WPNFs-GTB was significantly higher than that of uncoated bacteria, indicating that the protection of the WPNFs coating enabled the bacteria to tolerate such high acidity and alkalinity. Similarly, Cao et al. (2019) reported that the coating could increase the viability of probiotics at pH 2 and 11. The survival rates of probiotics in Lp-WPNFs and Lp-WPNFs-GTB at pH 2.0 were higher than those at pH 11.0, which may be closely related to the particular stability of WPNFs at pH 2.0 (Jiang et al., 2022; Liu, Chen, et al., 2024; Yang et al., 2022). At pH 2.0, WPNFs can reach lengths of 1–10 μm with large aspect ratios, while at pH 11.0 WPNFs exist as short fibrils (Jiang et al., 2022; Liu, Chen, et al., 2024), implying that larger aspect ratios will provide higher protection for bacteria. These improved storages, thermal, and pH stability will all contribute to the bacterial protection and expand its application in food processing. Therefore, it might be a useful technology for improving the survivability and accessibility of biological products.

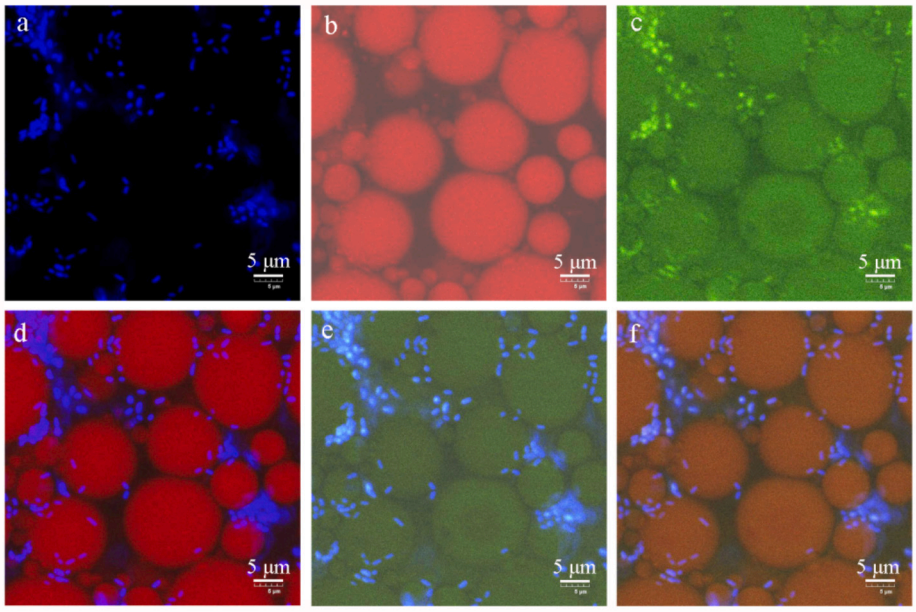

Fig. 4. CLSM images of Lp-WPNFs-GTB with GTB fraction of 40%. (a) the distribution of bacteria cells with blue fluorescence, (b) the distribution of GTB with red fluorescence, (c) the distribution of WPNFs with green fluorescence, (d) the superimposed effect of a and b, (e) the superimposed effect of a and c, (f) the superimposed effect of a, b and c. The insert scale bar is represented 5 μm with the magnification of 200 × . (For interpretation of the references to colour in this figure legend, the reader is referred to the web version of this article.)

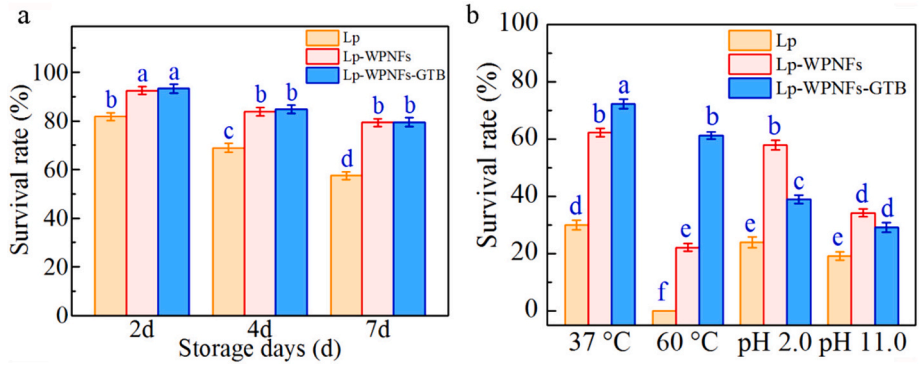

Fig. 5. Survival rates of probiotics in Lp, Lp-WPNFs and Lp-WPNFs-GTB against storage time at 4 °C and environmental stress. (a) Survival rates of probiotics in Lp, Lp-WPNFs and Lp-WPNFs-GTB during storage at 4 °C for different days. (b) Survival rates of probiotics in Lp, Lp-WPNFs and Lp-WPNFs-GTB under different heat and pH treatment (at 37 °C and 60 °C for 2 h, pH 2.0 and 11.0 for 2 h). Superscript letters indicate significant differences of $p < 0.05$.

3.3. Characterization of 3D printing ink

3.3.1. Rheological properties

In extrusion 3D printing, the printing inks are extruded layer by layer according to a pre-set design to obtain a 3D structure. The 3D printing ink plays a critical role, as it is needed to enable extrusion printing and maintain their shape accurately (Akkineni et al., 2022; Dick et al., 2020; Wang, Guo, et al., 2023). It is well accepted that rheological properties in terms of elastic modulus (G'), viscous modulus (G"), tan δ (G'/ G"), and viscosity, are the critical factors for the 3D printability as well as in the development of dysphagia foods (Bian et al., 2024; Lille et al., 2018; Liu et al., 2023).

G' and G", which are the crucial parameters to evaluate the ink adaptability, are shown in Fig. 6a. The higher G' value is related to the greater mechanical strength of the materials to self-support their own weight and maintain the shape after 3D printing (Cai et al., 2022; Wang, Guo, et al., 2023). The G" is the characterize related to the viscosity of materials, when the material is subjected to viscous deformation (irreversible) (Chen, Teng, Zhang, Mujumdar, and Li, 2023). For all CH printing inks, the G' and G" values increased with the frequency, and the G' values were consistently higher than the G" values over the entire frequency range, indicating that the CHs exhibited solid-like behavior. Comparing CH1, CH2 and CH3, both G' and G" increased significantly with increasing HG content. As previous studies have shown, HG can cause solidification during the printing by increasing the G' value of the ink (Bian et al., 2024; Lorenzo et al., 2013). Comparing CH2, CH4 and CH5, both G' and G" increased slightly with increasing WPI content. Similarly, increasing the WPI content can be used to increase the G' and G" values of composite hydrocolloids (Chow et al., 2021; Fan et al., 2022), and likewise, WPI could lessen the negative aspects of the pure lactose composite and benefiting the 3D printing process (Fan et al., 2022). Comparing CH6, CH2 and CH7, both G' and G" decreased with increasing FOS content, mainly because FOS interfered with the formation of the protein network, weakened the gel network with a reduced elastic behavior (Pachekrepapol et al., 2020). Comparing CH8, CH2 and CH9, both G' and G" decreased with increasing the Lp-WPNFs-GTB emulsion content.

Tan δ (G'/ G") is an indicator of the viscoelastic nature of gels. Tan δ

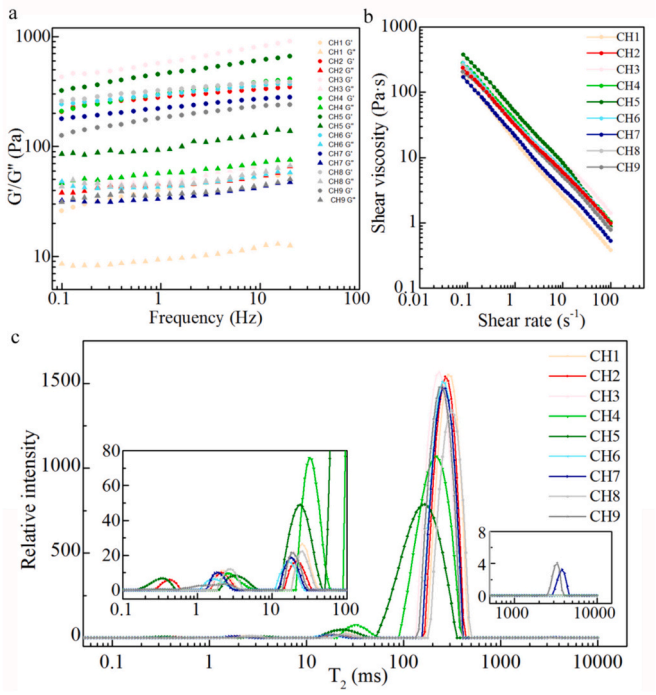

Fig. 6. The influence of components on rheological properties and Low-field NMR analysis. (a) storage modulus (G') and loss modulus (G") of CHs; (b) Shear viscosity as a function of shear rate; (c) Distributions of T_2 relaxation time of CHs.

< 1 indicates a predominantly elastic behavior, while Tan δ > 1 indicates a predominantly viscous behavior (Suebsaen et al., 2019). All CH samples had tan δ values of 0.08–0.34 (**Fig. S2**), suggesting an elastic-like behavior. In agreement with the results of the previous analyses, the elasticity of CHs was mainly provided by the addition of HG and WPI, and the effect of FOS on the tan δ value is not significant. Tan δ values in the range of 0.1–1.0 have been proposed as a rheological criterion for safe-swallowing of foods appropriate for elderly with dysphagia (Suebsaen et al., 2019). Therefore, it can be inferred from the tan δ value that CHs are suitable for use as 3D printing inks for dysphagia diets.

The extrudability is impacted by shear viscosity because shear stress is created at the nozzle during the 3D printing process. The ink with low viscosity exhibits stable extrusion, but it may lack sufficient mechanical support when stacked layer by layer. On the contrary, if the viscosity is high, it will be difficult to extrude (Bian et al., 2024; Wang, Guo, et al., 2023). All the CHs exhibited shear-thinning behavior (Fig. 6b and **Fig. S1**), which is considered an important property required for 3D printing and dysphagia dietary applications (Dick et al., 2020; Liu et al., 2023). While, the viscosity of the CHs increased with increasing HG content, this can be attributed to the fact that HG has a strong binding affinity with water, which reduces the water activity in CHs and increases the number of hydrogen bonds and physical cross-linking density between molecules (Bian et al., 2024). This result is consistent with the work of Akkineni et al. (2022) where a similar increase in viscosity was observed as the HG concentration in the blends increased.

The viscosity of CHs increased with increasing WPI content, similar to previous reports that gelation occurs with WPI and HG and the viscosity increases with their concentrations (Oliveira et al., 2020). The viscosity of CHs decreased with increasing FOS content, indicating that the addition of FOS provided a negative impact on the rheological parameters, which is due to FOS interfering with the formation of the protein networks (Pachekrepapol et al., 2020). The decrease in viscosity with the addition of FOS was also found in lactose-free functional yogurt (Pachekrepapol et al., 2020) and in Greek yogurt (Costa et al., 2019). The content of Lp-WPNFs-GTB emulsions had no significant effect on the viscosity of CHs.

3.3.2. *LF-NMR spectra of CHs*

The water state of the ink played an important role in the extrudability and mechanical properties of the ink (Bian et al., 2024). LF-NMR testing uses the spin-spin relaxation time (T_2) as the main indicator to analyze the different microenvironments in which protons are located (Wang, Guo, et al., 2023; Zhong et al., 2022). In general, a smaller T_2 value indicates a tighter bond between water and the matrix (Yang et al., 2018; Zhong et al., 2022). The peak (T_{21}) between 0.1 and 1 ms represents a monolayer of water tightly bound to amino or carboxyl groups in the matrix by hydrogen bonding; peak between 1 and 10 ms (T_{22}) and 10–100 ms (T_{23}) represent immobilized water that is weakly bound to the matrix; peak between 100 and 500 ms (T_{24}) represent partially immobilized water; and peaks >500 ms (T_{25}) represent free water (Cai et al., 2023; Wang, Guo, et al., 2023).

The LF-NMR results in Fig. 6c and **Table S1** were used to analyze the water state of the printed CHs. With lower T_2 value, the water in the sample is less free and more strongly bound to the solid phase (Bian et al., 2024). Three to four peaks were observed in the T_2 distribution spectrum of CHs; among them, the water population corresponding to T_{24} accounted for the largest proportion. In particular, CH2 and CH3 have an additional peak of T_{21} compared to CH1, indicating that the increase in HG content leads to an increase in tightly bound water. The shortened T_{23} and T_{24} indicate that HG has water-binding capacity and contributes to the gel network (Bian et al., 2024). The results indicated that HG is more effective in reducing water flow in the matrix space and promoting gel structure hydration, which is consistent with the rheological results of CHs (Ge et al., 2022). The lower water activity is beneficial for structural stability during the printing process and rapid solidification after printing (Bian et al., 2024).

CH5 with the shortened T_{23} and T_{24} compared to CH2, as well as increased A_{21}, A_{22} and A_{23}, suggested that WPI enhanced the immobilization of water in the hydrogel matrix (Xing et al., 2022). Comparing CH6, CH2 and CH7, the additional peak of T_{25} increased with increasing FOS content, indicating that the increase in FOS content leads to an increase in free water, which is also due to the fact that FOS interferes with the formation of the protein networks (Pachekrepapol et al., 2020) and reduces the binding capacity of free water. The Lp-WPNFs-GTB emulsion content had a similar effect, with an increase in content and the appearance of the T_{25} peak, suggesting that an increase in the Lp-WPNFs-GTB emulsion content leads to an increase in free water. These LF-NMR findings are consistent with the rheological characterization results described above.

3.3.3. *Texture profile analysis*

Texture testing has been used to simulate the chewing and swallowing process in the oral cavity (Wang, Zhang, et al., 2023). Dysphagia foods generally require customization in terms of hardness, adhesiveness, cohesiveness and springiness (Chen, Teng, Zhang, Bhandari, et al., 2023), and Table 2 lists the textural properties of CHs. Dysphagia foods should be soft with appropriate hardness values. All CHs presented a hardness of <50 g, which might facilitate them more suitable for people with dysphagia (Kan et al., 2023). The hardness of CHs was significantly affected by the content of HG, WPI, FOS and Lp-WPNFs-GTB with the first three factors significantly increasing the hardness and the last one significantly decreasing it. The increase in Lp-WPNFs-GTB content decreased the hardness of CHs, which may be due to probiotics breaking down WPI as a nitrogen source, and the decreasing trend was correlated with the the number of probiotics (Chen, Teng, Zhang, Bhandari, et al., 2023). Based on the results of rheological analysis, the hardness was directly related to the G' value, and a similar result was reported previously (Suebsaen et al., 2019).

Adhesiveness is defined as the energy required to overcome the adhesion force between the test sample and the test probe (Kan et al.,

Table 2
Texture profiles of CHs with different formulations.

Formula	Hardness (g)	Adhesiveness (mJ)	Cohesiveness	Springiness (mm)
CH1	22.77 ± 1.23e	0.15 ± 0.01e	0.67 ± 0.03f	2.31 ± 0.14e
CH2	25.12 ± 0.91d	0.27 ± 0.02bc	0.71 ± 0.03def	3.14 ± 0.14d
CH3	38.19 ± 1.89b	0.33 ± 0.01a	0.80 ± 0.01ab	4.10 ± 0.10b
CH4	26.52 ± 0.79 cd	0.14 ± 0.01e	0.76 ± 0.02bc	4.15 ± 0.12b
CH5	42.20 ± 0.38a	0.11 ± 0.02f	0.81 ± 0.01a	3.80 ± 0.06c
CH6	20.40 ± 0.99f	0.23 ± 0.02d	0.70 ± 0.02ef	4.96 ± 0.18a
CH7	27.11 ± 0.62 cd	0.29 ± 0.01b	0.75 ± 0.01 cd	4.20 ± 0.12b
CH8	28.03 ± 1.25c	0.27 ± 0.02bc	0.72 ± 0.02cde	3.86 ± 0.08c
CH9	20.76 ± 1.46f	0.26 ± 0.01c	0.67 ± 0.04f	3.76 ± 0.09c

Note: Different letters in the same column means significant differences ($p < 0.05$).

2023). High adhesiveness means that the tongue needs to exert more force during swallowing, which increases the risk of choking during swallowing (Suebsaen et al., 2019). The adhesiveness was strongly influenced by the content of HG, WPI and FOS, but was less affected by Lp-WPNFs-GTB, where an increase in HG and FOS content resulted in an increase, while WPI resulted in a decrease. This means that variations in HG and WPI content can be used to regulate the hardness and adhesiveness of CHs. The adhesiveness of CHs ranged from 0.11 to 0.33 mJ, indicating that it takes only a short time to leave the palate and teeth, making it suitable for dysphagia foods (Kan et al., 2023).

Cohesiveness is a characterization of the internal strength of food, and can be used to assess the ability of the material to keep continuous during 3D printing (Wang, Guo, et al., 2023). High cohesiveness indicates a strong internal bonding of the material, which prevents food from dispersing into small particles during swallowing, and facilitates safe swallowing (Wang, Zhang, et al., 2023). The cohesiveness was influenced by HG and WPI content but was less affected by FOS and Lp-WPNFs-GTB, where an increase in HG and WPI content resulted in an increase in cohesiveness. The increased cohesiveness indicated that an increase in HG and WPI content could enhanced the interparticle forces in CHs.

Springiness is an indication of the ability of the food to return to its original shape after being compressed or stretched (Kan et al., 2023). The increase in springiness with increasing HG content indicated that HG in CHs contributed more to the formation of a highly elastic gel network structure (Kan et al., 2023). The increase in WPI content accompanied by the decrease in springiness indicated that WPI in CHs contributed more to the formation of viscous gel network structures. In summary, the textural properties of CHs can be modulated by adjusting the content of HG and WPI.

3.4. 3D printing and characteristics

3.4.1. Evaluation of printability

Excellent printability can be evaluated in terms of smoothness, printing accuracy, and post-printing stability; good printability results in good print quality (Wang, Guo, et al., 2023). The printability of the ink was evaluated to optimize the ink formulation (Fig. 7a). The printing ink should be able to maintain the accurate printed shape, and also have sufficient mechanical strength to prevent collapse (Wang, Guo, et al., 2023). All the CH samples with shear-thinning behavior could be extruded from the tip of the nozzle, and the lower the G' value and shear viscosity is, the easier they are extruded, but the weak support capacity

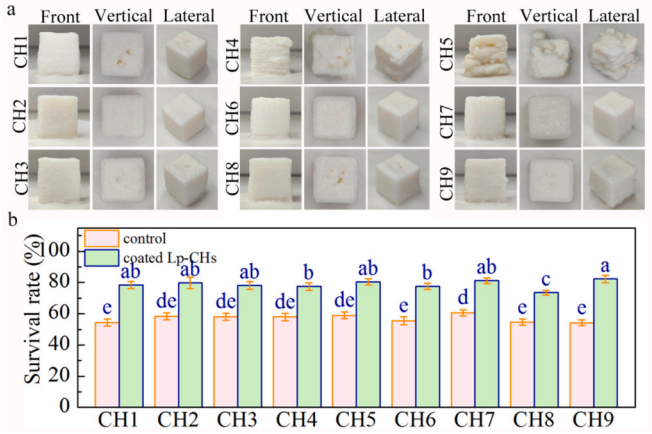

Fig. 7. The influence of component on 3D printing performance and survival rate of L. *plantarum*; (a) Optical images of 3D printing cubes with an edge length of 2.0 cm; (b) Survival rate of L. *plantarum*.

(Wang, Guo, et al., 2023).

In the HG gradient experiments, the studied groups were smoothly extruded during the 3D printing, and the materials formed target shapes by mutual adhesion. However, there were differences in their ability to maintain shape. The insufficient amount of HG (CH1) was easily to be extruded but the 3D printed cube deformed slightly and showed a fatter bottom. This may be due to the fact that CH1 had low G' and G", and was unable to support the subsequent deposition layers, leading to printing deviations (Xu et al., 2023). CH2 presented the best 3D printing precision with smooth surface and high printing accuracy, and good shape stability after printing, due to the increased G' and self-supporting ability by increasing the HG content. In comparison, further increase of HG content (CH3), the cube was printed with high accuracy but with a coarse surface, which was mainly due to the fact that both the higher G' value and the viscosity of the ink, which made the extrusion slightly more difficult. Similar results were found for the increasing the HG concentration in the printing ink, which resulted in better shape fidelity (Akkineni et al., 2022; Bian et al., 2024).

The effect of the amount of WPI on the 3D printing results was very significant. The increased content of WPI, the surface of the cube becomes rougher, which was mainly due to the fact that ink extrusion becomes difficult. The increase in WPI content improved the G', G", shear viscosity and reduced the adhesiveness resulting in the rough surface. The contents of FOS and Lp-WPNFs-GTB do not have a significant effect on the printability of 3D printing inks. The cube printed with CH2 presented the best result with high print resolution, smooth surfaces and stable shape. Combined with the results of the rheological and texturing properties, the interrelation between the G' value, viscosity, adhesiveness and cohesiveness of the 3D printing ink are key factors influencing the 3D printing effect (Wang, Guo, et al., 2023).

The accuracy and stability of CH2 printed cubes are characterized by the side length of the printed sample and its variation with storage time, as shown in Table S2. The length, width and height of the CH2 printed cube is at 20.0 ± 0.5 mm, which is a small difference compared with the set value of 20.0 mm. After 24 h of storage at 4 °C, the side lengths were all slightly smaller, mainly due to slight water loss (Wang, Guo, et al., 2023). The samples maintained a stable length and height without tipping or collapsing, indicating that CH2 has good printing accuracy and stability.

CH2 as the optimal formulation was used to test its printability on complex 3D structures. As shown in Fig. 8, the design details of letters and shapes printed by the CH2 formulation were displayed, with smooth surfaces and no fracture or collapse, which rendered the designed structures. Compared with traditional production methods, 3D printing has the advantages of convenience, speed, less material waste, and can

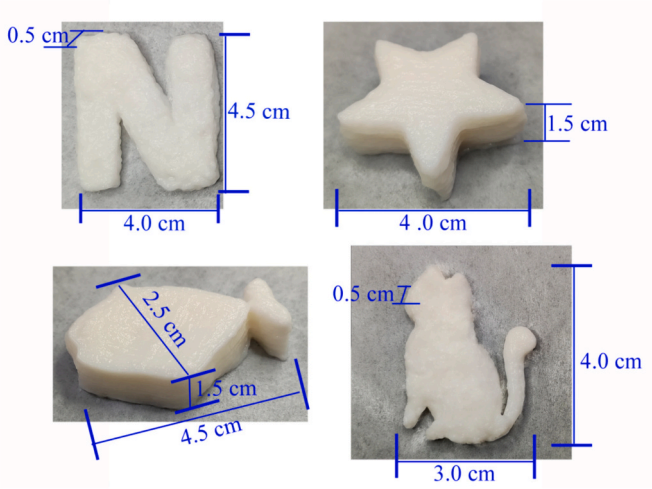

Fig. 8. The examples of 3D printed objects with CH2 (0.25 g HG, 1.25 g WPI, 0.75 g FOS, and 3.75 mL of Lp-WPNFs-GTB). The printing nozzle diameter is 0.84 mm, extrusion cavity temperature 45 °C and print speed 20 mm/s.

produce a variety of complex structures in a shorter time (Bian et al., 2024). The finished products printed with CH2 have the advantages of personalized shape, rich in nutritious, probiotics and prebiotics, making them an attractive diet for dysphagia patients.

3.4.2. Survival rate for 3D printing process

In order to obtain the potential health benefit, the viability and concentration of live probiotic microorganisms in the food products are very important (Mahmoodi Pour et al., 2022). The daily dose of probiotics is considered to be 10^9–10^{11} CFU (Muzzafar & Sharma, 2018). Hence, a therapeutic minimum of 100 g of 10^6–10^8 CFU/g is generally satisfy the daily requirement (Muzzafar and Sharma, 2018).

The effect of the 3D printing process on the survival rate of probiotics was investigated by estimating the viable cell counts before and after 3D printing. The difference between the control and treated groups was only whether the Lp was coated with WPNFs or not. The survival rate of probiotics in the control group without significant difference after the 3D printing process (Fig. 7b), indicating that there is no significant difference in the protective effect between HG, WPI, FOS and Pickering emulsions on the probiotic during 3D printing. And the lower survival rates in the control group is due to the fact that the mechanical shear at the nozzle during extrusion (Yoha et al., 2021) and the temperature of the extrusion cavity (45 °C) resulting in lower bacterial viability (Liu, Li, et al., 2020). There was no significant difference in survival rates between the treated groups, which once again confirms this conclusion. However, the difference between the control and treated group was significant, and the survival rate of probiotics in 3D printed samples could reach 73.54% to 81.15%, which was much higher than that in the control group, ranging from 52.24% to 60.66%, confirming that the WPNFs coating on the surface of the probiotics significantly improved the survival rate of the probiotics.

The viable cell counts in the treated group were found to range from 7.30 to 9.92 log CFU/g, with CH2 reaching 8.0 log CFU/g, which is in line with the recommended level of 10^6–10^8 CFU/g (Muzzafar and Sharma, 2018), showing that the 3D-printed CHs can be successfully used as a vehicle to deliver probiotics.

3.4.3. IDDSI test

IDDSI provides a global standard and test methods for evaluating diets designed for people with dysphagia (Wang, Zhang, et al., 2023). According to the IDDSI framework, there are 8 levels (0–7) of foods and liquids intended for dysphagia diets (https://iddsi.org/Framework). Although the rheological and textural properties of CHs could assist in the optimization of easy-to-swallow formulations, it could not directly characterize the easy-to-swallow level of the product. Accordingly, the fork pressure and spoon tilt tests (Fig. 9) were applied to evaluate the level of the 3D printed CHs as dysphagia foods.

3D printed cubes were evaluated by a fork pressure test, which could distinguish between levels of five and six in the IDDSI framework (Wang, Zhang, et al., 2023). The gap distance between the fork's prongs is 4 mm, which meets the requirement of a safe size for food particles of 2–4 mm before swallowing (Liu et al., 2023). In the fork pressure tests, all CHs were easily squashed with little pressure, without the thumb nail blanching to white. The CHs were able to pass through the prongs of the fork and formed a clear pattern on the surface that did not return to its original shape when the pressure was released. The results indicated that CHs belonged to level 5-minced & moist diet labeled in the IDDSI framework.

The spoon tilt test can be used to test the stickiness and cohesiveness of the samples, which could distinguish the levels four and five in the IDDSI framework (Wang, Zhang, et al., 2023). As shown in Fig. 9, all CHs could hold its shape on the spoon, when the spoon was tilted, the food on the spoon easily slip off with very little left or lightly flicked. If the sample does not slide off and most of it remains on the spoon, indicating that the sample is too sticky, which will increase the chocking risk. This indicated that CHs belonged to level 5-minced & moist diet labeled in IDDSI framework, and the compositional content of CHs within the selection range did not affect their level.

4. Conclusions

In this study, WPNFs were coated on the bacterial surface via bio-interfacial supramolecular self-assembly to improve the probiotic survival rate in stressful environments such as strong acid (pH 2.0) and alkali (pH 11.0), high temperature conditions, and 3D printing process. CHs exhibited solid-like and shear-thinning behavior with Tan δ values ranging from 0.08 to 0.34, which meets a rheological criterion for safe-swallowing of dysphagia foods. HG and WPI as carrier matrix have the ability to bind water and form gel networks, and their addition can be adjusted to change their textural properties and enhance their 3D printing printability. The 3D printing ink CH2 containing 0.25 g of HG, 1.25 g of WPI, 0.75 g of FOS and 3.75 mL of Lp-WPNFs-GTB provide optimal printability with surviving cells up to 8.0 log CFU/g. The structures can be accurately printed with a smooth and flat surface without tipping or collapsing. IDDSI tests indicated that the CHs were classified as level 5-minced & moist dysphagia diet. This study would provide valuable information on the preparation of appetite provoking dysphagia foods enriched with probiotics by 3D printing. Future studies will aim to evaluate the effects of this food on gastrointestinal digestion to understand the contribution of probiotics to human health.

CRediT authorship contribution statement

Ye Zhang: Writing – original draft, Methodology, Data curation. **Yexuan Wang:** Writing – original draft, Software, Data curation, Conceptualization. **Xiaohan Dai:** Software, Formal analysis. **Ying Li:** Validation, Software, Methodology, Formal analysis. **Bin Jiang:** Writing – review & editing, Project administration. **Dongmei Li:** Formal analysis, Data curation. **Chunhong Liu:** Writing – review & editing, Supervision, Funding acquisition, Conceptualization. **Zhibiao Feng:** Supervision, Project administration, Conceptualization.

Declaration of competing interest

The authors declare that they have no known competing financial interests or personal relationships.

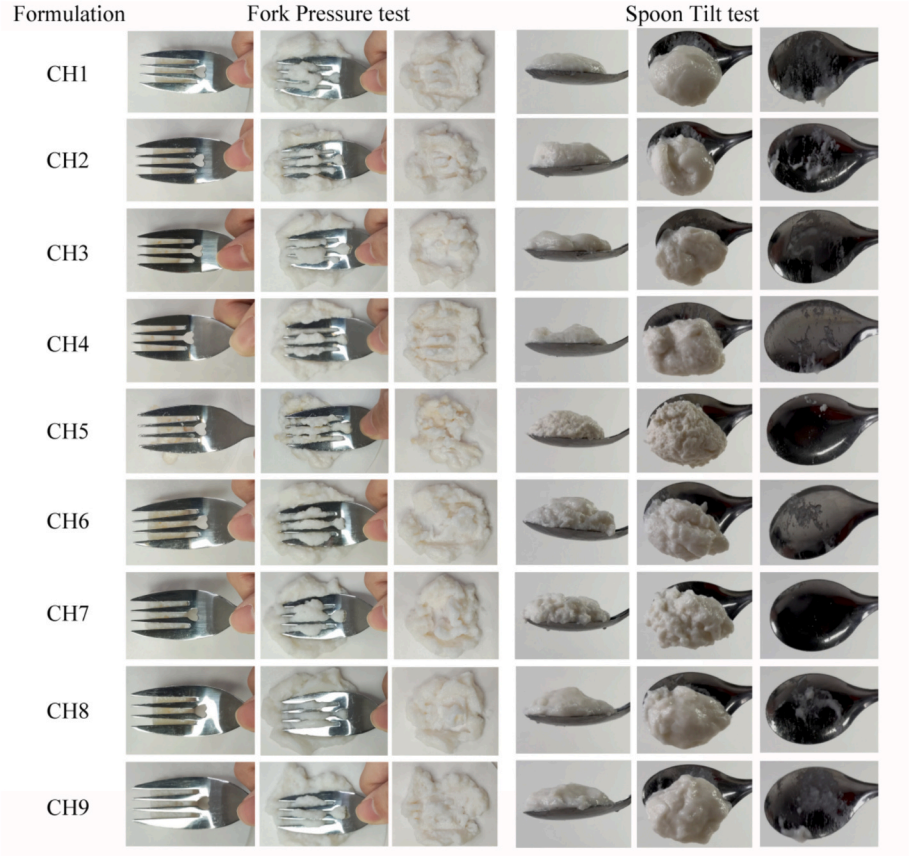

Fig. 9. Evaluation of the easy-to-swallow performance of 3D printed CHs by IDDSI test.

Data availability

Data will be made available on request.

Acknowledgements

This research was funded by Heilongjiang Nature Scientific Foundation Project (LH2020C029).

Appendix A. Supplementary data

Supplementary data to this article can be found online at https://doi.org/10.1016/j.foodchem.2024.140720.

References

Abbasi, S., Rafati, A., Hosseini, S. M. H., Roohinejad, S., Hashemi, S. S., Hashemi Gahruie, H., & Rashidinejad, A. (2023). The internal aqueous phase gelation improves the viability of probiotic cells in a double water/oil/water emulsion system. *Food Science & Nutrition, 11*(10), 5978–5988.

Akkineni, A. R., Elci, B. S., Lode, A., & Gelinsky, M. (2022). Addition of high acyl gellan gum to low acyl gellan gum enables the blends 3D bioprintable. *Gels, 8*(4), 199.

An, D., Ban, Q., Du, H., Wang, Q., Teng, F., Li, L., & Xiao, H. (2022). Nanofibrils of food-grade proteins: Formation mechanism, delivery systems, and application evaluation. *Comprehensive Reviews in Food Science and Food Safety, 21*(6), 4847–4871.

An, D., Zhai, S., & Li, L. (2023). Characteristics of soy protein hydrolysate nanofibrils and their stabilization mechanism for Pickering emulsion: Interfacial properties, rheology and stability. *LWT - Food Science and Technology, 189*, Article 115473.

Bian, M., Jiang, S., Liu, S., Zhang, L., Miao, S., Zhou, F., & Zheng, B. (2024). Fish gelatin and gellan gum mixture as edible ink for 3D printing. *Journal of Food Engineering, 362*, Article 111762.

Cai, Q., Zhong, Y., Huang, Q., Huang, G., & Lu, X. (2023). Co-incorporation of probiotics into 3D printed custard cream with hydrophilic and hydrophobic bioactives. *Food Hydrocolloids, 142*, Article 108809.

Cai, Q., Zhong, Y., Xu, M., Huang, Q., & Lu, X. (2022). 3D printed high oil custard cream: Effects of whey protein isolate, hydroxypropylated starch and carrageenan on physicochemical properties and printing performance. *LWT - Food Science and Technology, 156*, Article 113039.

Cao, W., Guan, S., Tristanto, N. A., Yuan, Y., Li, Z., Tong, Y., & Hua, X. (2024). Tributyrin microcapsule prepared by ultrahigh methoxylated pectin combination with maltodextrin: The characterization, gastrointestinal digestion, and fecal fermentation behavior. *Food Hydrocolloids, 148*, Article 109505.

Cao, Y., & Mezzenga, R. (2019). Food protein amyloid fibrils: Origin, structure, formation, characterization, applications and health implications. *Advances in Colloid and Interface Science, 269*, 334–356.

Cao, Z., Wang, X., Pang, Y., Cheng, S., & Liu, J. (2019). Biointerfacial self-assembly generates lipid membrane coated bacteria for enhanced oral delivery and treatment. *Nature Communications, 10*(1).

Chen, J., Teng, X., Zhang, M., Bhandari, B., Adhikari, B., & Yu, D. (2023). 5D food printing with color change induced by probiotic growth in a starch-protein-based gel system. *Food and Bioprocess Technology, 16*(10), 2304–2314.

Chen, Q., Ma, H., Yuan, Y., Han, X., Zhu, J., & Zhang, H. (2017). Rheaological behavior of high acyl gellan gum solution at gel point. *International Journal of Food Properties, 20*(53), S2332–S2341.

Chen, X., Teng, X., Zhang, M., Mujumdar, A. S., & Li, J. (2023). Functional changes in 5D printed starch-based gel systems caused by spontaneous growth of probiotics. *Food and Bioprocess Technology, 17*(8), 2470–2482.

Chow, C. Y., Thybo, C. D., Sager, V. F., Riantiningtyas, R. R., Bredie, W. L. P., & Ahrné, L. (2021). Printability, stability and sensory properties of protein-enriched 3D-printed lemon mousse for personalised in-between meals. *Food Hydrocolloids, 120*, Article 106943.

Costa, M. F., Pimentel, T. C., Guimaraes, J. T., Balthazar, C. F., Rocha, R. S., Cavalcanti, R. N., … Cruz, A. G. (2019). Impact of prebiotics on the rheological characteristics and volatile compounds of Greek yogurt. *LWT - Food Science and Technology, 105*, 371–376.

Dick, A., Bhandari, B., Dong, X., & Prakash, S. (2020). Feasibility study of hydrocolloid incorporated 3D printed pork as dysphagia food. *Food Hydrocolloids, 107*, Article 105940.

Donovan, J. D., Bauer, L., Fahey, G. C., & Lee, Y. (2017). In vitro digestion and fermentation of microencapsulated tributyrin for the delivery of butyrate. *Journal of Food Science, 82*(6), 1491–1499.

Fan, F., Li, S., Huang, W., & Ding, J. (2022). Structural characterization and fluidness analysis of lactose/whey protein isolate composite hydrocolloids as printing materials for 3D printing. *Food Research International, 152*, Article 110908.

Fan, Y., Peng, G., Pang, X., Wen, Z., & Yi, J. (2021). Physicochemical, emulsifying, and interfacial properties of different whey protein aggregates obtained by thermal treatment. *LWT- Food Science and Technology, 149*, Article 111904.

Gao, Z., Zhao, J., Huang, Y., Yao, X., Zhang, K., Fang, Y., … Yang, H. (2017). Edible Pickering emulsion stabilized by protein fibrils. Part 1: Effects of pH and fibrils concentration. *LWT - Food Science and Technology, 76*, 1–8.
Ge, Z., Yin, D., Li, Z., Chen, X., & Dong, M. (2022). Effects of commercial polysaccharides stabilizers with different charges on textural, rheological, and microstructural characteristics of set yoghurts. *Foods, 11*(12), 1764.
Guo, N., Ma, Y., Zhang, F., Zhu, G., Yu, Z., Dai, H., & Wang, Z. (2023). Effect of pH on the thermal gel properties of whey protein isolate-high acyl gellan gum. *Journal of the Science of Food and Agriculture, 103*(7), 3346–3352.
Guo, Q., Tang, J., Li, S., Qiang, L., Chang, S., Du, G., Yue, T., & Yuan, Y. (2022). Lactobacillus plantarum 21805 encapsulated by whey protein isolate and dextran conjugate for enhanced viability. *International Journal of Biological Macromolecules, 216*, 124–131.
Han, B., Chen, P., Guo, J., Yu, H., Zhong, S., Li, D., Liu, C., Feng, Z., & Jiang, B. (2023). A novel intelligent indicator film: Preparation, characterization, and application. *Molecules, 28*(8), 3384.
Han, M., Yang, S., Song, J., & Gao, Z. (2024). Layer-by-layer coated probiotics with chitosan and liposomes demonstrate improved stability and antioxidant properties in vitro. *International Journal of Biological Macromolecules, 258*, Article 128826.
Jiang, B., Yue, H., Fu, X., Wang, J., Feng, Y., Li, D., Liu, C., & Feng, Z. (2024). One-step high efficiency separation of prolyl endopeptidase from aspergillus Niger and its application. *International Journal of Biological Macromolecules, 271*, Article 132582.
Jiang, F., Pan, Y., Peng, D., Huang, W., Shen, W., Jin, W., & Huang, Q. (2022). Tunable self-assemblies of whey protein isolate fibrils for Pickering emulsions structure regulation. *Food Hydrocolloids, 124*, Article 107264.
Kamada, A., Herneke, A., Lopez-Sanchez, P., Harder, C., Ornithopoulou, E., Wu, Q., … Lendel, C. (2022). Hierarchical propagation of structural features in protein nanomaterials. *Nanoscale, 14*(6), 2502–2510.
Kan, X., Dai, Z., Chen, D., Zeng, X., & Fan, X. (2023). High internal phase emulsion stabilized by whey protein isolate-gum Arabic Maillard conjugate: Characterization and application in 3D printing. *Food Hydrocolloids, 145*, Article 109137.
Kang, S. N., Hong, S. S., Lee, M. K., & Lim, S. J. (2012). Dual function of tributyrin emulsion: Solubilization and enhancement of anticancer effect of celecoxib. *International Journal of Pharmaceutics, 428*(1–2), 76–81.
Kim, W. S., Han, G. G., Hong, L., Kang, S. K., Shokouhimehr, M., Choi, Y. J., & Cho, C. S. (2019). Novel production of natural bacteriocin via internalization of dextran nanoparticles into probiotics. *Biomaterials, 218*, Article 119360.
Kwak, S., Robinson, S. J., Lee, J. W., Lim, H., Wallace, C. L., & Jin, Y.-S. (2022). Dissection and enhancement of prebiotic properties of yeast cell wall oligosaccharides through metabolic engineering. *Biomaterials, 282*, Article 121379.
Lille, M., Nurmela, A., Nordlund, E., Metsä-Kortelainen, S., & Sozer, N. (2018). Applicability of protein and fiber-rich food materials in extrusion-based 3D printing. *Journal of Food Engineering, 220*, 20–27.
Lin, S., Wu, F., Zhang, Y., Chen, H., Guo, H., Chen, Y., & Liu, J. (2023). Surface-modified bacteria: Synthesis, functionalization and biomedical applications. *Chemical Society Reviews, 52*(19), 6617–6643.
Liu, C., Wang, Y., Dai, X., Zhang, Y., Yang, Y., Jiang, B., … Feng, Z. (2024). Post-self-assemble of whey protein isolation nanofibrils and its contribution to the stability of Pickering emulsion. *Food Hydrocolloids, 151*, 109766.
Liu, G., Li, W., Qin, X., & Zhong, Q. (2020). Pickering emulsions stabilized by amphiphilic anisotropic nanofibrils of glycated whey proteins. *Food Hydrocolloids, 101*, Article 105503.
Liu, H., Gong, J., Chabot, D., Miller, S. S., Cui, S. W., Zhong, F., & Wang, Q. (2018). Improved survival of lactobacillus zeae LB1 in a spray dried alginate-protein matrix. *Food Hydrocolloids, 78*, 100–108.
Liu, S., Wu, J., Wu, Z., Alugongo, G. M., Zahoor Khan, M., Li, J., … Cao, Z. (2022). Tributyrin administration improves intestinal development and health in pre-weaned dairy calves fed milk replacer. *Animal Nutrition, 10*, 399–411.
Liu, Z., Bhandari, B., & Zhang, M. (2020). Incorporation of probiotics (Bifidobacterium animalis subsp. Lactis) into 3D printed mashed potatoes: Effects of variables on the viability. *Food Research International, 128*, Article 108795.
Liu, Z., Chen, X., Dai, Q., Xu, D., Hu, L., Li, H., Hati, S., Chitrakar, B., Yao, L., & Mo, H. (2023). Pea protein-xanthan gum interaction driving the development of 3D printed dysphagia diet. *Food Hydrocolloids, 139*, Article 108497.
Liu, Z., Chen, X., Li, H., Chitrakar, B., Zeng, Y., Hu, L., & Mo, H. (2024). 3D printing of nutritious dysphagia diet: Status and perspectives. *Trends in Food Science & Technology, 147*, Article 104478.
Lorenz, T., Iskandar, M. M., Baeghbali, V., Ngadi, M. O., & Kubow, S. (2022). 3D food printing applications related to dysphagia: A narrative review. *Foods, 11*(12), 1789.
Lorenzo, G., Zaritzky, N., & Califano, A. (2013). Rheological analysis of emulsion-filled gels based on high acyl gellan gum. *Food Hydrocolloids, 30*(2), 672–680.
Mahmoodi Pour, H., Marhamatizadeh, M. H., Fattahi, H., & Di Maro, A. (2022). Encapsulation of different types of probiotic bacteria within conventional/multilayer emulsion and its effect on the properties of probiotic yogurt. *Journal of Food Quality, 2022*, 1–12.
Mazziotta, C., Tognon, M., Martini, F., Torreggiani, E., & Rotondo, J. C. (2023). Probiotics mechanism of action on immune cells and beneficial effects on human health. *Cells, 12*(1), 184.
Meng, Y., Wei, Z., & Xue, C. (2022). Protein fibrils from different food sources: A review of fibrillation conditions, properties, applications and research trends. *Trends in Food Science & Technology, 121*, 59–75.
Muzzafar, A., & Sharma, V. (2018). Microencapsulation of probiotics for incorporation in cream biscuits. *Journal of Food Measurement and Characterization, 12*(3), 2193–2201.
Nezamdoost-Sani, N., Khaledabad, M. A., Amiri, S., & Mousavi Khaneghah, A. (2023). Alginate and derivatives hydrogels in encapsulation of probiotic bacteria: An updated review. *Food Bioscience, 52*, Article 102433.
Ok, S., Yilmaz, E., & Demirel Zorba, N. N. (2024). Preparation and characterization of 3D printed objects based on different kefir gels. *Food Biophysics, 19*(2), 453–470.
Oliveira, S. M., Fasolin, L. H., Vicente, A. A., Fuciños, P., & Pastrana, L. M. (2020). Printability, microstructure, and flow dynamics of phase-separated edible 3D inks. *Food Hydrocolloids, 109*, Article 106120.
Pachekrepapol, U., Somboonchai, N., & Krimjai, W. (2020). Physicochemical, rheological, and microbiological properties of lactose-free functional yogurt supplemented with fructooligosaccharides. *Journal of Food Processing and Preservation, 45*(1).
Qiu, L., Zhang, M., Bhandari, B., Chitrakar, B., & Chang, L. (2023). Investigation of 3D printing of apple and edible rose blends as a dysphagia food. *Food Hydrocolloids, 135*, Article 108184.
Ramos, C. L., Thorsen, L., Schwan, R. F., & Jespersen, L. (2013). Strain-specific probiotics properties of lactobacillus fermentum, lactobacillus plantarum and lactobacillus brevis isolates from Brazilian food products. *Food Microbiology, 36*(1), 22–29.
Stepnaya, O., Begunova, E., Tsfasman, I., Tul'skaya, E., Streshinskaya, G., Naumova, I., & Kulaev, I. (2004). The mechanism of action of the extracellular bacteriolytic enzymes of *Lysobacter* sp. on gram-positive bacteria: The role of the cell wall anionic polymers of target bacteria. *Microbiology, 73*(4), 479–485.
Suebsaen, K., Suksatit, B., Kanha, N., & Laokuldilok, T. (2019). Instrumental characterization of banana dessert gels for the elderly with dysphagia. *Food Bioscience, 32*, Article 100477.
Sun, C., Wang, S., Yang, L., & Song, H. (2023). Advances in probiotic encapsulation methods to improve bioactivity. *Food Bioscience, 52*, Article 102476.
Sun, P., Zhang, Y., Zhang, Y., Feng, Z., Lee, S. J., & Serventi, L. (2022). Antimicrobial activity of tofu whey and steam blanching pea water for enhancement of shelf-life of 3D printed mashed potatoes. *Food Bioscience, 50*, Article 102049.
Wang, D., Guo, J., Wang, Y., Yang, Y., Jiang, B., Li, D., Feng, Z., & Liu, C. (2023). Whey protein isolate nanofibrils as emulsifying agent to improve printability of Cheddar cheese for 3D printing. *Food Hydrocolloids, 142*, Article 108807.
Wang, X., Zhang, M., Mujumdar, A. S., & Li, J. (2023). Easy-to-swallow mooncake using 3D printing: Effect of oil and hydrocolloid addition. *Food Research International, 164*, Article 112404.
Wei, Z., & Huang, Q. (2019). Assembly of iron-bound ovotransferrin amyloid fibrils. *Food Hydrocolloids, 89*, 579–589.
Xing, X., Chitrakar, B, Hati, S, Xie, S, Li, H, Li, C, … Mo, H. (2022). Development of black fungus-based 3D printed foods as dysphagia diet: Effect of gums incorporation. *Food Hydrocolloids, 123*, 107173.
Xu, D., Liu, Z., An, Z., Hu, L., Li, H., Mo, H., & Hati, S. (2023). Incorporation of probiotics into 3D printed Pickering emulsion gel stabilized by tea protein/xanthan gum. *Food Chemistry, 409*, Article 135289.
Yadav, M. K., Kumari, I., Singh, B., Sharma, K. K., & Tiwari, S. K. (2022). Probiotics, prebiotics and synbiotics: Safe options for next-generation therapeutics. *Applied Microbiology and Biotechnology, 106*(2), 505–521.
Yang, F., Zhang, M., Prakash, S., & Liu, Y. (2018). Physical properties of 3D printed baking dough as affected by different compositions. *Innovative Food Science & Emerging Technologies, 49*, 202–210.
Yang, X., Song, Y., Guo, R., Xu, H., & Jin, C. (2024). Structural modification of whey protein nanofibrils by a multiround induction pathway for enhancing the stability of Pickering emulsions. *Food Hydrocolloids, 150*, Article 109703.
Yang, Y., Jiao, Q., Wang, L., Zhang, Y., Jiang, B., Li, D., Feng, Z., & Liu, C. (2022). Preparation and evaluation of a novel high internal phase Pickering emulsion based on whey protein isolate nanofibrils derived by hydrothermal method. *Food Hydrocolloids, 123*, Article 107180.
Yoha, K. S., Anukiruthika, T., Anila, W., Moses, J. A., & Anandharamakrishnan, C. (2021). 3D printing of encapsulated probiotics: Effect of different post-processing methods on the stability of Lactiplantibacillus plantarum (NCIM 2083) under static in vitro digestion conditions and during storage. *LWT - Food Science and Technology, 146*, Article 111461.
Yuan, Y., Yin, M., Zhai, Q., & Chen, M. (2022). The encapsulation strategy to improve the survival of probiotics for food application: From rough multicellular to single-cell surface engineering and microbial mediation. *Critical Reviews in Food Science and Nutrition*, 1–17.
Zhang, Y., Liang, S., Zhang, J., Chi, Y., Tian, B., Li, L., Jiang, B., Li, D., Feng, Z., & Liu, C. (2020). Preparation of whey protein isolate nanofibrils by microwave heating and its application as carriers of lipophilic bioactive substances. *LWT - Food Science and Technology, 125*, Article 109213.
Zhang, Y., Xie, Y., Liu, H., McClements, D. J., Cheng, C., Zou, L., … Liu, W. (2022). Probiotic encapsulation in water-in-oil high internal phase emulsions: Enhancement of viability under food and gastrointestinal conditions. *LWT - Food Science and Technology, 163*, Article 113499.
Zhong, Y., Cai, Q., Huang, Q., & Lu, X. (2022). Application of LF-NMR to characterize the roles of different emulsifiers in 3D printed emulsions. *Food Hydrocolloids, 133*, Article 107993.